Experimental and Computational Studies Investigating Trehalose Protection of HepG2 Cells from Palmitate-Induced Toxicity

Sukit Leekumjorn,* Yifei Wu,† Amadeu K. Sum,* and Christina Chan†
*Department of Chemical Engineering, Virginia Polytechnic Institute and State University, Blacksburg, Virginia; and †Department of Chemical Engineering and Material Science, Michigan State University, East Lansing, Michigan

ABSTRACT Understanding the mechanism of saturated fatty acid-induced hepatocyte toxicity may provide insight into cures for diseases such as obesity-associated cirrhosis. Trehalose, a nonreducing disaccharide shown to protect proteins and cellular membranes from inactivation or denaturation caused by different stress conditions, also protects hepatocytes from palmitate-induced toxicity. Our results suggest that trehalose serves as a free radical scavenger and alleviates damage from hydrogen peroxide secreted by the compromised cells. We also observe that trehalose protects HepG2 cells by interacting with the plasma membrane to counteract the changes in membrane fluidity induced by palmitate. The experimental results are supported by molecular dynamics simulations of model cell membranes that closely reflect the experimental conditions. Simulations were performed to understand the specific interactions between lipid bilayers, palmitate, and trehalose. The simulations results reveal the early stages of how palmitate induces biophysical changes to the cellular membrane and the role of trehalose in protecting the membrane structure.

INTRODUCTION

Non-esterified long-chain free fatty acids (FFAs) are major sources of cellular energy (1) and essential components in triglycerides, cholesteryl esters, prostaglandins, and phospholipid syntheses (2,3). There have been numerous reports on the toxic effects of fatty acids on model cells in vitro. Andrade et al. showed that both saturated and unsaturated fatty acids exert toxic effects on melanoma cells through the loss of membrane integrity or DNA fragmentation (4). Lima et al. evaluated the toxicity of various fatty acids on Jurkat (T-lymphocytes) and Raji (B-lymphocytes) cells (5) and found a positive correlation between the toxicity and the chain length and number of double bonds in the fatty acids. Their experiments identified palmitate among the most toxic of the fatty acids. FFAs, especially saturated fatty acids, can cause cell death in many types of cells, including pancreatic β-cell (6,7), cardiomyocytes (8,9), and hepatocytes (10–12).

Most of the research up until now on the mechanism of cell death focused on the production of potential or toxic intermediates, such as stearoyl-CoA desaturase 1 (13–15), acids from omega oxidation (16,17), reactive oxygen species (ROS), ceramide (18,19), reduced mitochondrial potential (8), and reduction of mitochondrial Bcl-2/Bax ratio (11). Recent studies in our lab suggest that palmitate can cause lipotoxicity in liver cells through increased production of hydrogen peroxide (H_2O_2) and hydroxyl (*OH) radicals (12). Measurements indicated that the cytotoxicity was not completely prevented upon treatment with mitochondrial complex inhibitors or free radical scavengers. This suggests that mechanisms other than ROS production in the mitochondria may be contributing to the toxicity of palmitate. Therefore, we investigated the possibility that palmitate-induced toxicity may be due to hydrophobic effects on the cellular membrane. Fatty acids are known to have toxic and fusogenic effects on cells (20,21). The mechanism by which fatty acids exert cytotoxicity has been identified as the detergent-effect (22). According to this hypothesis, ionized fatty acid micelles solubilize membrane lipids or proteins and disrupt the physical and functional integrity of cell membranes (20,21).

Identifying chemical agents to prevent or reverse the effect of fatty acid induced cellular toxicity has been a major focus of research in the past decades. Studies have suggested that saturated and unsaturated fatty acids have different effects on toxicity. For example, there has been evidence indicating that dietary oleic acid can protect endothelial cells against hydrogen peroxide-induced oxidative stress and reduce the susceptibility of LDLs to oxidative modifications (23–25). Similarly, we found that oleic acid does not induce the same level of cytotoxicity as palmitic acid in HepG2 cells at similar concentrations (12) and the addition of oleic acid reduces the cytotoxicity induced by palmitate (26). In another related study, Kinter et al. investigated the protective role of unsaturated FFA in oxygen-induced toxicity of hamster fibroblasts and found that monounsaturated FFA increased cell survival as compared to saturated and polyunsaturated FFAs (27). Furthermore, it has been shown that unsaturated FFAs rescued palmitate-induced apoptosis by converting palmitate into triglycerides (13). Recently, Natali et al. investigated the effects of various types of FFAs in glial cells and found that oleic acid was a potent inhibitor of fatty acid and cholesterol synthesis (28). In recent years, it has been established experimentally that trehalose has a stabilizing effect on biological membranes (29) by protecting cells from dehydration, heat, and cold (30–32). Moreover, evidence is mounting

Submitted August 28, 2007, and accepted for publication November 20, 2007.

Address reprint requests to Christina Chan, Tel.: 517-432-4530; E-mail: krischan@egr.msu.edu.

Editor: Jennifer Linderman.

© 2008 by the Biophysical Society
0006-3495/08/04/2869/15 $2.00

doi: 10.1529/biophysj.107.120717

suggesting that trehalose acts as an antioxidant, possibly serves as a free radical scavenger (33–35), and inhibits the peroxidation of unsaturated fatty acids by heat or oxygen radicals (35,36). In addition, trehalose has been found to protect yeast cells and cellular proteins from damage by oxygen radicals during oxidative stress (37). In light of the role trehalose plays in the stabilization of cells, we investigated whether trehalose is protective in the presence of palmitate, and if so, we aimed at understanding how trehalose protects against palmitate-induced toxicity.

Therefore, to gain insight into how trehalose interacts with liver cells (human hepatocellular carcinoma cell line, HepG2 cells) in the presence of palmitate, we performed a series of experimental and computational measurements. The experimental measurements focused on determining the influence of palmitate and trehalose on the fate of HepG2 cells, and the computational part aimed at interpreting and understanding the experimental results, shedding light into the role of palmitate and trehalose in the toxicity of HepG2 cells. Insight into these mechanisms will add to our understanding of processes (i.e., metabolic, signaling, and biophysical) that are altered by palmitate. We found that palmitate decreased the cellular membrane fluidity of HepG2 cells. The addition of trehalose to palmitate cultures prevented this lowering in membrane fluidity. Thus, we found that trehalose protects also against palmitate-induced toxicity in liver cells. This study represents the first attempt to obtain a comprehensive understanding of the biochemical and biophysical processes leading to and resulting from the toxicity of palmitate on cells.

EXPERIMENTAL MATERIALS AND METHODS

Cell culture

Human hepatocellular carcinoma cell line, HepG2 (American Type Culture Collection, Manassas, VA), was cultured in Dulbecco's modified Eagle's medium (DMEM, Invitrogen, Carlsbad, CA) containing 10% fetal bovine serum (American Type Culture Collection) and 2% penicillin-streptomycin (Invitrogen). They were seeded in six-well plates and incubated at 37°C in humidified atmosphere containing 10% CO_2. After cells reached confluence, the media were replaced with 2 ml control medium (4% fatty-acid free bovine serum albumin, or BSA) or palmitate (0.7 mM with 4% BSA) and changed every 24 h. The BSA level used was close to physiological conditions (38). A quantity of 0.7 mM FFAs was employed in this study because the plasma FFA levels in the obese and type 2 diabetic patients have been reported to be approximately this level (39–42). Experiments were conducted after 48 h of treatment. To determine the optimal amount of trehalose to add, we performed a dose-response in HepG2 cells with trehalose ranging from 0 to 0.2 mM.

Cytotoxicity assay

Cell viability was assessed by lactate dehydrogenase (LDH) leakage through the membrane into the medium. The cell culture supernatant from control and palmitate-treated cultures were tested after 48 h of incubation for the presence of LDH (LDH_{medium}) using an LDH assay kit (Roche Applied Science, Indianapolis, IN). Cells were washed with phosphate-buffered saline (PBS) and lysed with 1% triton-X 100 for 12 h at 37°C. The cell lysate was then centrifuged at 5000 *g* for 10 min and tested for LDH activity (LDH_{triton}). The LDH released was normalized to the total LDH, given by

$$\%LDH_{\text{release}} = \frac{LDH_{\text{medium}}}{LDH_{\text{medium}} + LDH_{\text{triton}}} \times 100. \quad (1)$$

Membrane fluidity

Two different stearic-acid derivatives were used to detect changes in the membrane fluidity, 5-*n*-doxylstearic acid (5-*n*-SASL) and 16-*n*-doxylstearic acid (16-*n*-SASL) (Invitrogen, Carlsbad, CA). The 5-*n*-SASL probe monitors the portion of the membrane closest to the lipid headgroups, while the 16-*n*-SASL reflects changes in the middle/end of the lipid hydrocarbon chains (43).

A stock solution of the spin labeled stearic acids at 10^{-3} M was prepared in dimethyl-sulfoxide and the aliquots stored at −20°C. Immediately before use, the stock solution was thawed and diluted 50 times with PBS. Preliminary experiments were conducted to confirm that the spin-label solution did not affect the cell viability. Cell suspensions collected after Trypsin-EDTA (GIBCO, Billings, MT) exposure were centrifuged and the pellets were resuspended in spin label solution and kept on ice. The labeled cell suspensions were then transferred to a flat cell and placed in the cavity of the electron paramagnetic resonance (EPR) spectrometer (model No. ESP-300E X-band; Bruker AXS, Madison, WI). The microwave power was set at 15.8 mW, the modulation frequency at 100 kHz, and the modulation amplitude at 2.53 G. For indexes of membrane fluidity, we evaluated the values of the outer and inner hyperfine splitting ($2T_\perp$ and $2T_\parallel$ in Gauss, respectively) in the EPR spectra for 5-*n*-SASL. The order parameter was calculated from $2T_\perp$ and $2T_\parallel$ by

$$S = \frac{T_\parallel - (T_\perp + C)}{T_\parallel + (2T_\perp + C)} \times 1.66, \quad (2)$$

where $C = 1.4 - 0.053(T_\parallel - T_\perp)$. In the EPR spectra for 16-*n*-SASL, we used the peak height ratio ($h_o/h - 1$) for an index of the membrane fluidity (44,45), where h_o and $h - 1$ are the heights of the central and high-field peaks, respectively. The greater the values of the order parameter and peak height ratio, the lower the freedom of motion of the spin labels in the membrane bilayers, indicating lower membrane fluidity (43).

Liposome preparation and DSC measurement

To correlate the fluidity measurements to our computational studies, a simpler model cell membrane also was used. Liposomes (multilamellar vesicles) were prepared by the thin film method according to the protocol from Avanti Polar Lipids. The lipid 1,2-dioleoyl-*sn*-glycero-3-phosphocholine (DOPC, Avanti Polar Lipids, Alabaster, AL) and palmitic acid (Sigma-Aldrich, St. Louis, MO), obtained in chloroform stock solutions, were mixed in appropriate amounts in a glass tube. After vortexing, the solvent was dried under nitrogen. This formed a thin lipid film on the inside wall of the glass tube. The film was dried in a freeze-dryer to ensure complete evaporation of chloroform. Deionized water was added into the tube before it was placed in a bath sonicator for 10 min. Differential scanning calorimetry (DSC) analysis were performed on the liposomes samples at a scan rate of 1°C/min. Samples containing 20 mg/ml of lipid and 10 μL of liposome suspensions were used. DOPC was used in these experiments because its phase transition temperature (~−19°C) allowed us to obtain clean and clear DSC scans, whereas POPC (one of the lipids used in the simulations studies) has a phase transition temperature near the normal melting point of water (−2°C for POPC), which causes severe interference in obtaining reliable data.

SIMULATION DETAILS

To gain insight into how palmitate induces cytotoxicity, we used MD simulations to investigate the role palmitate and

trehalose play in the structure and integrity of lipid bilayers (model biological membranes). The lipid bilayers used here are equimolar 1-palmitoyl-2-oleoyl-*sn*-glycero-3-phosphocholine/1-palmitoyl-2-oleoyl-*sn*-glycero-3-phosphoethanolamine (POPC/POPE) bilayers with a total of 288 lipid molecules evenly distributed in each leaflet (System 1 in Table 1). This mixed bilayer was chosen for these studies because it represents the main phospholipid constituents of HepG2 cells (46). Note that other major lipid constituents (e.g., cholesterol) were not included in these simplified model bilayers. Combinations of palmitate and trehalose were introduced into the lipid bilayer systems. The structure of the molecules considered is shown in Fig. S1 in the Supplementary Material.

To mimic the exposure of palmitate to cells with and without trehalose, a palmitate molecule was inserted into the middle of the aqueous phase of previously equilibrated lipid bilayers (System 3 in Table 1). For the systems with trehalose, a concentration of ~5 wt % trehalose was used in the aqueous phase (System 4 in Table 1). A low trehalose concentration was chosen because it represents the range of concentrations reported in cryopreservation, lyophilization, and other modeled membrane-trehalose studies (30,47–49). To obtain a statistical analysis of the diffusion process, 10 sets of simulations were performed on each bilayer with and without trehalose. We set up these simulations with a single palmitate molecule in the aqueous phase because of aggregation at higher concentrations (see Fig. S2 in the Supplementary Material) and experimental evidence that shows the free unbound palmitate in solution (~10 nM) are largely responsible for the biophysical changes to the membrane (50). Note that BSA, used in the experiments to prevent palmitate aggregation, is not considered in the simulations. Because palmitate is a relatively long molecule (in its fully stretched, 16-carbon-long conformation), it was necessary to consider systems with a large aqueous phase (40 waters per lipid), so that the palmitate molecule would interact with only one of the bilayer interfaces at any given time.

TABLE 1 Composition for lipid bilayers

System	Trehalose	Palmitate	Ensemble
1	—	—	*NPT*
2	30*	—	*NPT*
3	—	1*	*NPT*
4	30*	1*	*NPT*
5	—	16†	*NPT*
6	—	32†	*NPT*
7	—	48†	*NPT*
8	—	64†	*NPT*
9	—	16†	NP_zAT‡
10	—	32†	NP_zAT‡
11	—	48†	NP_zAT‡
12	—	64†	NP_zAT‡

All systems contain 144 lipids per leaflet with 40 waters per lipid. Each leaflet contains an equal number of POPC and POPE.

*Molecules inserted in the aqueous phase.

†Molecules embedded in the bilayer.

‡Compressibility set to zero in the *x*- and *y*-directions.

Experimental studies have shown that moderate to high concentrations of palmitate induce significant structural changes to the bilayer, including membrane swelling (51), membrane fusion (52,53), and degradation of membrane integrity (52,54). To understand the effect of these phenomena, two sets of simulations were proposed to explain the global and local effect of palmitate on the membranes (see Fig. S3 for pictorial representation). For the global effect, *NPT* simulations were performed. Here the simulations captured the effect of large membrane structures, because the bilayer surface was allowed to adjust as palmitate molecules were embedded into the bilayer. To avoid aggregation of palmitate in the aqueous phase, the bilayer structures were constructed to have various concentrations of palmitate embedded into the bilayer before equilibration (Systems 5–8 in Table 1). Simulations of these systems were used to address the overall changes of the membrane structure in the presence of palmitate. For the local effect, the changes in bilayer structure are limited to a specific portion of the membrane that is concentrated with palmitate. Here, NP_zAT (constant surface area) simulations were performed (surface area of the bilayer constrained to that without palmitate). Similarly, palmitate molecules were embedded in the bilayers before the start of the simulations (Systems 9–12 in Table 1). The goal of these latter studies was to investigate the membrane swelling induced by palmitate, which may eventually lead to membrane deformation or formation of ordered domains that alter the membrane fluidity.

The force-field for POPC, POPE, and water are consistent with those employed in previous studies (55–57), which includes intramolecular parameters for bonds, angles, proper dihedral, and improper dihedral. The Ryckaert-Bellemans potential was used for the torsion potential of the lipid hydrocarbon chains (58). Nonbonded interactions were described by the parameters from Berger et al. (59–61) and partial atomic charges were obtained from Chiu et al. (62). The united-atom representation was used for the methyl/methylene groups in the acyl chains of both POPC and POPE. For POPE, the hydrogen atoms in the amine group are explicitly listed in the topology. The optimized potential for liquid simulations (OPLS-AA) force field was used for trehalose (63). Palmitate was modeled in the protonated state and described using parameters derived from the lipid force field. The carboxylic acid group was based on the parameters of glutamic acid, which were available from the GROMOS force field (64). The single-point charge model was adopted for water (65).

Simulations were performed at 310 K (see (66) for more details on the parameters used in the simulations). A timestep of 2 fs was used for all simulations. Coulombic and van der Waal cutoff interactions were at 1.0 nm. Long-range electrostatic interactions were corrected with the particle-mesh Ewald method (67,68) (0.12 nm for the grid size,

fourth-order spline interpolation, and real-space cutoff at 1.0 nm). Periodic boundary conditions were applied in all directions. Trajectories were collected every 2 ps. All simulations were performed with the GROMACS 3.3.1 software package (69,70) (single-precision mode) in parallel using Virginia Tech's System X (dual 2.3 GHz Apple Xserve G5) (71).

EXPERIMENTAL RESULTS

Palmitate cytotoxicity and trehalose protective role

We previously found that palmitate-induced toxicity led to ROS production in HepG2 cells (12), but its effect was not prevented upon treating with ROS scavengers. During oxidative stress, yeast cells produce trehalose to protect themselves from damage by oxygen radicals (37). Therefore, we evaluated the effect of trehalose on palmitate-induced toxicity in HepG2 cells. The level of cytotoxicity was measured by the relative amount of LDH released in the medium. The control consisted of HepG2 cells exposed to DMEM with 4% BSA. From Fig. 1, our measurements indicate that palmitate significantly increased the amount of LDH released, relative to the control. As the concentration of trehalose increased, the LDH released reduced significantly. This protective effect reached a maximum at a trehalose concentration of 0.13 mM, whereupon further increase in the trehalose concentration was detrimental to the HepG2 cells. Although the mechanism of trehalose-induced toxicity is not a focus of this study, we infer from previous studies, including our own, that trehalose preferentially binds to the membrane and possibly causes surface modifications that may affect cell activity (72–77). As it will be demonstrated from our computational studies, we found that trehalose can induce local hydrophobic/hydrophilic domains along the bilayer interface, a membrane reorganization process which may have potentially detrimental effects. Based on these findings, a trehalose concentration of 0.13 mM was optimum for alleviating the palmitate-induced toxicity in HepG2 cells and it was used in all subsequent experiments.

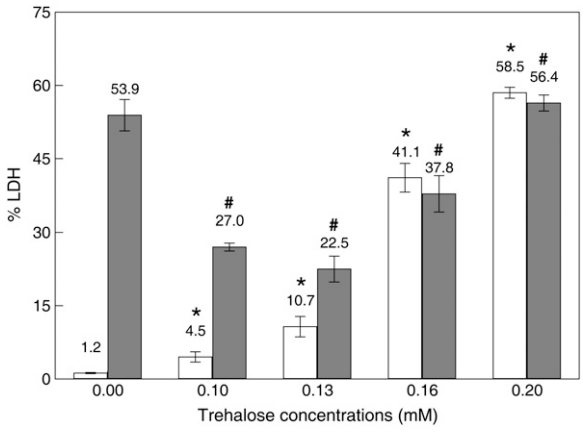

FIGURE 1 Effect of trehalose on the HepG2 cells cytotoxicity in response to palmitate. Confluent HepG2 cells in bovine serum albumin (BSA) medium were exposed to 0.7 mM palmitate in the presence of different concentrations of trehalose. The LDH released was measured after 48 h. Open and shaded bars represented the effect of trehalose alone or the mixtures of trehalose/palmitate, respectively. Note that the first shaded bar shows the effect of palmitate alone. Error bars are standard deviation of three independent experiments. The symbols * and # indicate statistical difference from control and palmitate, respectively ($p < 0.05$).

Trehalose on H_2O_2 release

We previously identified H_2O_2 as one of the ROS species involved in the palmitate-induced toxicity of hepatoma cells. To determine whether trehalose protected HepG2 cells by scavenging H_2O_2, the measured H_2O_2 released into the medium was normalized to total cellular protein. As shown in Fig. 2, 48 h of palmitate exposure enhanced H_2O_2 release into the medium, while trehalose significantly reduced the H_2O_2 release in the presence of palmitate. The results suggest that trehalose protects the cells in part by reducing H_2O_2 release.

Membrane fluidity for HepG2 cells

Since palmitate is hydrophobic, there may be nonspecific cytotoxic effects due to its hydrophobicity. It has been established experimentally that trehalose has a stabilizing effect on biological membranes (78), therefore we investigated the changes in cellular membrane structure upon exposure to palmitate in the presence and absence of trehalose. The cellular membrane fluidity of HepG2 cells in the presence of palmitate or trehalose was measured by EPR. The EPR spectra of the spin-label agents were used to detect changes in the freedom of motion of the lipids in the cell membrane, thus

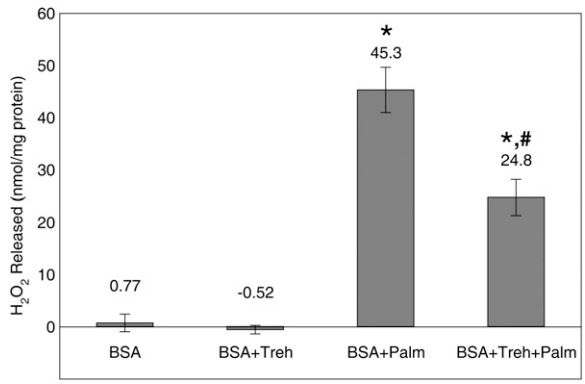

FIGURE 2 Effects of trehalose and palmitate on H_2O_2 release. Confluent HepG2 cells in BSA medium were treated with 0.7 mM palmitate (*Palm*) with or without 0.13 mM trehalose (*Treh*) for 48 h. The H_2O_2 released into the medium was measured and normalized to total cellular protein. Error bars are standard deviation of three independent experiments. The symbols * and # indicate statistical difference from control and palmitate, respectively ($p < 0.05$).

providing a measure of the membrane fluidity. The membrane fluidity of HepG2 cells were measured after 48 h of exposure to palmitate, trehalose, and combinations thereof. The control was HepG2 cells exposed to DMEM with 4% BSA. Using 16-*n*-SASL as a probe to monitor the ordering of the lipid tails near the center of the bilayer core, we observed a greater peak height ratio for the palmitate-treated cells as compared to the control, which correlated with reduced freedom of motion of the spin labels in the membrane. This indicates a decrease in membrane fluidity of the cells treated with palmitate for 48 h, as shown in Fig. 3 *a*. The exposure of HepG2 cells to trehalose had an insignificant effect on the bilayer core region since trehalose is excluded from the bilayer. The interaction of trehalose with the membrane is only at the surface of the bilayer. Treating HepG2 cells with trehalose and palmitate increased the peak height ratio. This suggests that a complex interaction exists between the cellular membrane, palmitate, and trehalose. Similarly, using 5-*n*-SASL as a probe to monitor the lipid carbons near the lipid headgroups, we observed that the presence of trehalose in the palmitate-treated cells increased the fluidity near the surface of the membrane (see Fig. 3 *b*).

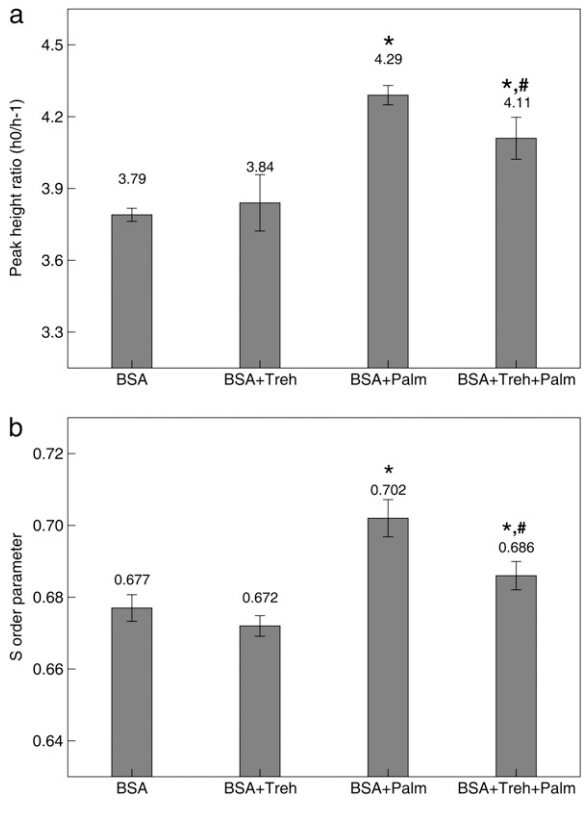

FIGURE 3 Effect of palmitate exposure on cellular membrane fluidity. Cells were treated with 0.7 mM palmitate in the presence or absence of 0.13 mM trehalose for 48 h. The cellular membrane fluidity was measured using EPR. (*a*) Values are peak height ratio for 16-*n*-SASL-labeled HepG2 cells. (*b*) Values are order parameter for 5-*n*-SASL-labeled HepG2 cells. Error bars are standard deviation of four independent experiments. The symbols * and # indicate statistical difference from control and palmitate, respectively ($p < 0.05$).

To corroborate the membrane fluidity results, we measured the phase transition temperature of DOPC liposomes by DSC measurements. The DSC thermographs for DOPC liposomes with varying mole fractions of palmitate (see Fig. 4) showed that the phase transition temperature of the DOPC liposomes increased with increasing concentration of palmitate. This suggests that palmitate increase the ordering of the phospholipids in the liposomes, which correlates with the decrease in membrane fluidity measured by EPR.

COMPUTATIONAL RESULTS

Based on the experimental results, exposure of healthy cells to palmitate resulted in cytotoxicity, while the presence of trehalose partially alleviated the negative effect by palmitate. As such, there must be a complex interaction between palmitate, trehalose, and the cell membrane to enable this process to occur. Based on the large number of hydroxyl groups present in trehalose, we hypothesize that the distribution of hydrogen bonds among trehalose, phospholipid, and palmitate is the key in determining the protective mechanism. Therefore, MD simulations were performed on lipid bilayers to elucidate the possible mechanisms of palmitate-induced toxicity and the mechanism by which trehalose protects cells from palmitate-induced toxicity. It should be noted that while MD simulations to investigate the biological function of trehalose (72–77) and palmitate (79,80), separately, are present in the literature, their combined role is absent.

Palmitate dynamics

The initial stage of cell exposure to palmitate is modeled by introducing a single palmitate molecule in the aqueous phase of previously equilibrated bilayers with and without

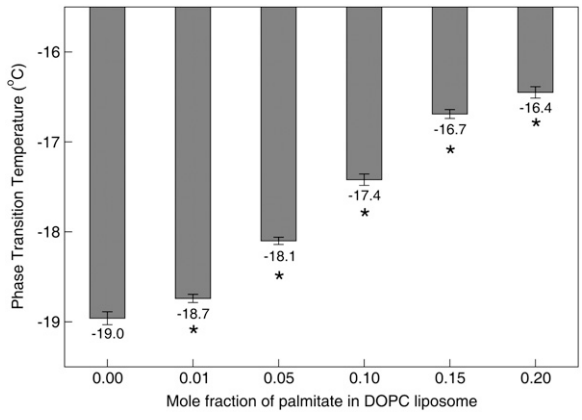

FIGURE 4 Phase transition temperature of DOPC liposomes containing palmitate. The phase transition was measured with DSC. Error bars are standard deviation of three independent experiments. The symbol * indicates statistical difference from control, 0% palmitate ($p < 0.01$).

trehalose. Snapshots of the two systems at the start of the simulation are shown in Fig. 5. To obtain a statistical sampling of the palmitate penetration into the bilayer, 10 sets of simulations were performed for each system with different starting configurations and initial velocities. All simulations lasted 40 ns regardless of the time when palmitate penetrated the bilayer. Fig. 5, *b* and *d*, show representative trajectories of palmitate along the simulation (trajectory is traced by the position of the central carbon atom in the palmitate tail). As seen in the figure, palmitate can penetrate the bilayer within the simulation time considered. Eight of the ten simulations resulted with palmitate in the bilayer and palmitate remained in the aqueous phase for the duration of the simulations. For the simulations with trehalose, similar results were obtained. The observed penetration of palmitate in the bilayer is consistent with experimental studies that demonstrated that palmitate can be readily incorporate into the hydrophobic region of the bilayer (81,82).

The following observations were made from the simulations containing palmitate in the absence of trehalose. Initially in the aqueous phase, palmitate freely diffuses through the water molecules. Due to the hydrophobic nature of palmitate, entropic forces drive palmitate to migrate toward the bilayer core region (hydrophobic environment). As palmitate approaches the bilayer interface, numerous interactions must occur before the hydroxyl group of palmitate (H-donor) can favorably interact with the lipid oxygen atoms (H-acceptor) through hydrogen bonding. Note that the lipid oxygen atoms are those in the phosphate and carbonyl groups. First, at least two hydrogen-bond pairs, one between water (H-donor) and lipid oxygen atoms (H-acceptor), and another between the palmitate hydroxyl group (H-donor) and water (H-acceptor) must be broken for the palmitate to interact with the lipids, a process that requires a substantial amount of energy. Second, since the bilayer contains both POPC and POPE, an additional hydrogen bond between the amine groups of POPE (H-donor) and neighboring lipid oxygen atoms (H-acceptor) must be broken as well, if palmitate penetrates to the bilayer near POPE. Finally, the hydrophobic nature of palmitate is the driving force bringing palmitate closer to the bilayer interface and eventually into the bilayer core; nevertheless, the bilayer interface is hydrophilic and poses a barrier for palmitate to penetrate into the bilayer core. For these reasons, palmitate is often not readily incorporated into the bilayer core as it approaches the interface. This is illustrated in the trajectory shown in Fig. 5 *b*, where palmitate frequently interacts with the lipid interface before penetrating the bilayer. Once the alignment and interactions of palmitate at the interface are favorable, palmitate penetrates the bilayer with the hydrocarbon tail first. This is also seen from Fig. 5 *b*, where

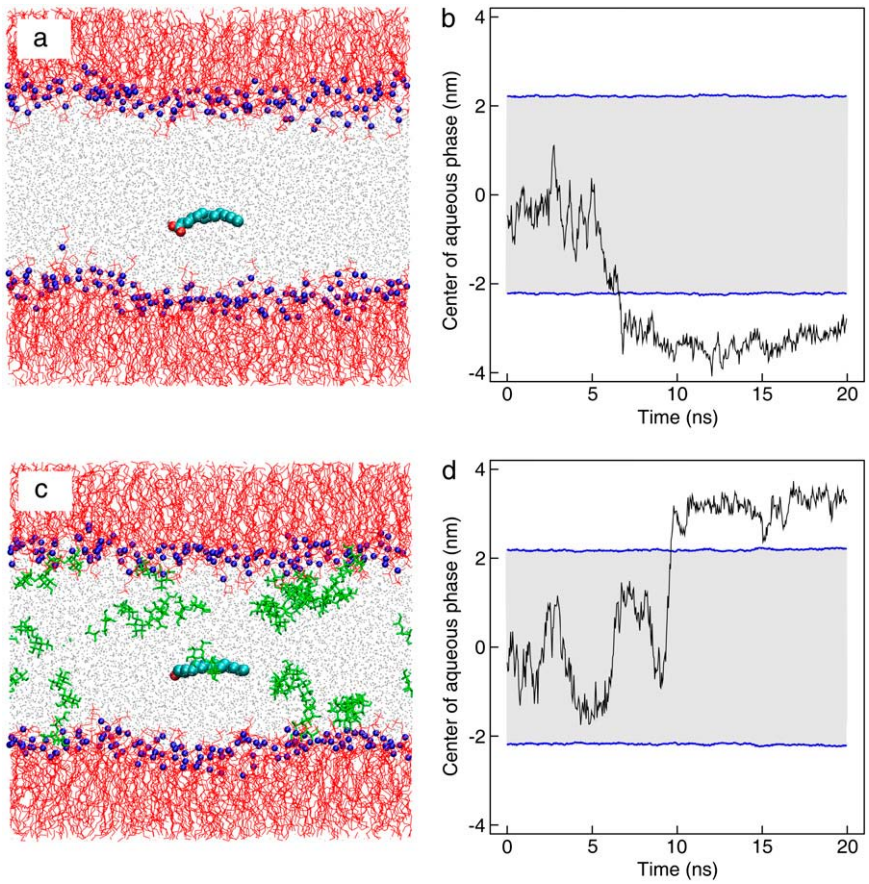

FIGURE 5 Starting structure of POPC/POPE bilayer with one palmitate inserted into the aqueous phase. Bilayers are modeled (*a*) without and (*c*) with trehalose. Colored molecules are POPC/POPE headgroup (*blue*), lipid tails (*red*), water (*gray*), trehalose (*green*), and palmitate (*cyan*). See Table 1 for composition. The dynamics of palmitate, represented by the position of central carbon atom in its tail, are shown in panels *b* and *d*. Blue horizontal lines correspond to the average position of the phosphorus atoms of POPC and POPE along the interface and are used to identify the interface. Gray area denote the aqueous regions. The position $z = 0$ corresponds to middle of the aqueous phase.

the palmitate trajectory remains almost stationary before crossing the interface and then quickly moving into the bilayer core. For lipid bilayers containing trehalose, the interactions of palmitate appeared to be much more complex, as the exchange of hydrogen bonds among lipids, trehalose, and palmitate have significant affect on the dynamics of the system.

Hydrogen-bond analysis

To investigate the protective role of trehalose on palmitate-induced toxicity, we correlated the number of hydrogen bonds between the bilayer lipids and palmitate up to the penetration time. The H-donors consisted of the palmitate hydroxyl group and the POPE amine group. The lipid and palmitate oxygen atoms were the H-acceptors. A hydrogen bond is defined according to the criteria suggested by Brady and Schmidt, with the distance between the donor and acceptor within 0.35 nm and the angle donor-hydrogen-acceptor between 120 and 180° (83). The penetration time is the time at which palmitate crosses the interface from the aqueous phase into the bilayer. In the absence of trehalose, palmitate penetrates the bilayer in shorter penetration time and forms more hydrogen bonds with the lipids than in the presence of trehalose. In the latter case, trehalose competes with palmitate for hydrogen bonds with the lipids, and thus trehalose can interfere with the interactions between the lipids and palmitate. Therefore, longer penetration time and fewer hydrogen bonds between the lipids and palmitate are expected. From the 20 simulations considered (10 with and 10 without trehalose), 16 showed palmitate penetrating into the bilayer within 40 ns of simulation. As shown in Fig. 6 *a*, the data does not seem to correlate with the number of hydrogen bonds (lipid-palmitate) and the penetration time. This suggests that the probability of palmitate penetrating the bilayer and interacting with the lipids and trehalose are more complex than initially proposed.

Following a similar approach, we correlated the number of hydrogen bonds between trehalose and palmitate up to the penetration time to provide insight into how trehalose may prevent palmitate-induced toxicity. Here, the H-donors and H-acceptors consisted of trehalose and palmitate hydrogens and oxygen atoms in the hydroxyl group, respectively. The results, shown in Fig. 6 *b*, demonstrate a direct correlation between the number of hydrogen bonds and the penetration time, suggesting that trehalose may be directly interacting with palmitate. Therefore, it is possible that, by interfering with the interaction of palmitate with the bilayer lipids, trehalose reduces the probability of palmitate-inducing toxicity.

An extensive hydrogen-bond analysis was carried out to investigate the interactions between lipids, trehalose, and palmitate. Here, a correlation was made between the penetration time and the number of hydrogen bonds present in the system. From Fig. 6 *b*, shorter penetration time was observed for systems with fewer hydrogen-bond interactions between

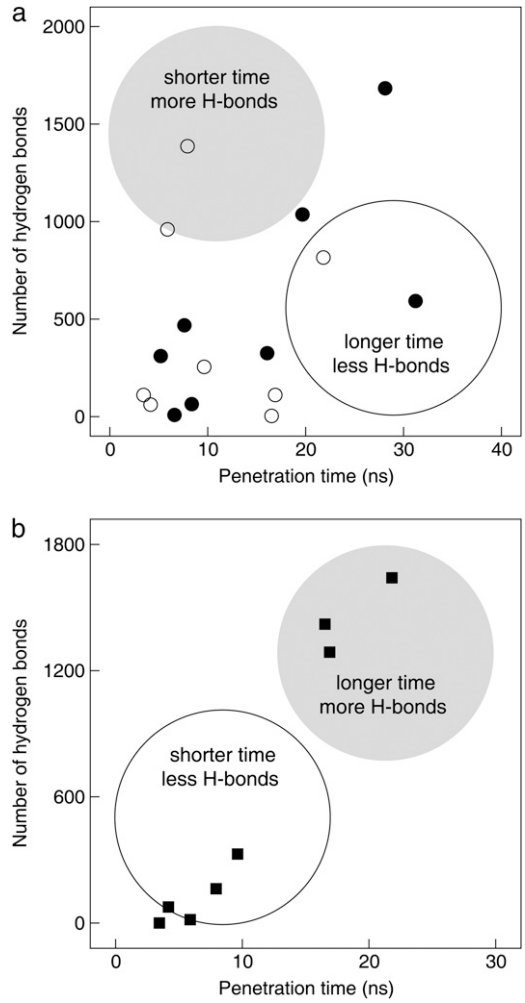

FIGURE 6 Correlation between the number of hydrogen bonds and palmitate penetration time. Closed and opened circles shown in panel *a* are the number of hydrogen bonds between lipid headgroups and palmitate for bilayers without and with trehalose, respectively. Squares shown in panel *b* are the number of hydrogen bonds between palmitate and trehalose. Highlighted circular areas are the regions in which we speculate the results to lie.

palmitate and trehalose. This suggests that, without trehalose, palmitate should penetrate more quickly into the bilayer. However, we see from the results that the penetration times are about the same for the systems with and without trehalose. Since the penetration of palmitate is dependent upon the lipid molecules exposed to the aqueous phase, we investigated the bilayer interface to explain the results. Since the bilayers consisted of two types of lipids, with POPE acting as an H-donor, the intermolecular H-bond distribution between lipids (the amine groups as H-donors and the lipid oxygen atoms as H-acceptors) may provide insight into this inconsistency. To accomplish this task, we calculated the H-bond distribution in the bilayer interface at the time of penetration. Note that the interface is one to which palmitate penetrates through. For clarity and discussion purposes, four bilayers

without trehalose and four bilayers with trehalose were selected. Fig. 7 shows the intermolecular hydrogen-bond distribution between lipids at the time of palmitate penetration. The penetration time and location are indicated in the figure. The first observation from the plots is that palmitate penetrates the bilayer in regions with fewer H-bonds between lipids. The void regions in the plots generally represent the choline headgroup in POPC molecules exposed to the aqueous phase. Note that the choline groups have three methyl groups, which are hydrophobic in nature. These facts and observations led us to conclude that palmitate, a hydrophobic molecule, prefers to penetrate the bilayer through hydrophobic

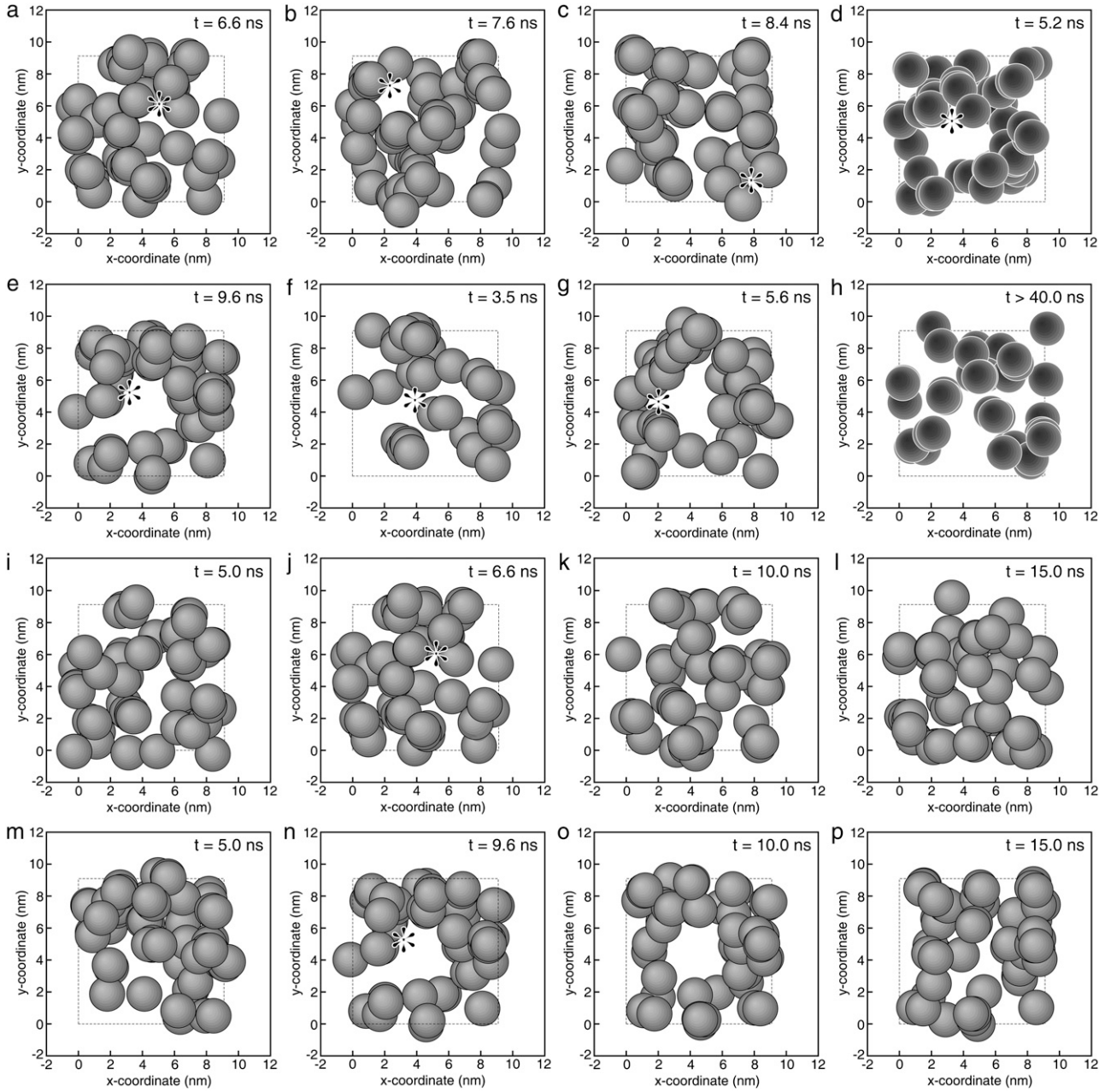

FIGURE 7 Snapshots of the hydrogen-bond distribution on a bilayer leaflet during the time of palmitate penetration for bilayers without (*a–d*) and with trehalose (*e–h*) and over the course of simulations for bilayers without (*i–l*) and with trehalose (*m–p*). Circles represent the location of intermolecular hydrogen bonds between the amine groups of POPE and neighboring lipid oxygen atoms. For bilayers considered with and without trehalose, the majority shows uniform hydrogen-bond distributions (*shaded circles* in *a–c* and *e–g*). Inconsistent hydrogen-bond distributions are shown in dark shading (*d* and *h*). Over the course of the simulation, the snapshots show uniform hydrogen-bond distributions for a bilayer without trehalose (*i–l*). Significant changes in the distribution are observed for bilayers with trehalose (*m–p*). Outlined square boxes are the approximate bilayer surface. The penetration time and location (*) are shown in each figure.

regions. Secondly, the H-bond distributions are more random in systems without trehalose and become more localized in systems with trehalose. As a result, there are fewer but large hydrophobic regions exposed to the aqueous phase for systems containing trehalose, implying that trehalose has the ability to modify the bilayer surface (84,85). Furthermore, the penetration time varies depending on the palmitate location and distribution of H-bonds on the surface. As seen in Fig. 7 *d* for a system without trehalose, the H-bond distributions are very similar to those systems containing trehalose (Fig. 7, *e–g*); as a result, palmitate penetrates the bilayer with the shortest amount of time. On the other hand, palmitate does not penetrate the bilayer surface with large hydrophobic regions, as shown in Fig. 7 *h*, mainly because palmitate interacts with trehalose in the aqueous phase, thus preventing palmitate from approaching the bilayer surface.

To verify that trehalose has the ability to modify the bilayer surface, we monitored the intermolecular H-bond distribution between lipids over the course of the simulation. The time considered for this analysis was between 5 and 15 ns. Selected snapshots are shown in Fig. 7, *i–p*, for bilayers with and without trehalose. It is evident from Fig. 7, *i–l* (system without trehalose), that the H-bond distributions are random throughout the bilayer surface, even at the time when palmitate penetrates the bilayer. A different behavior is observed for systems with trehalose, where significant changes in the H-bond distribution are observed before and after the penetration time, as shown in Fig. 7, *m–p*. A shift in H-bond distribution may have resulted from the multiple hydrogen bonds between trehalose and lipid oxygen atoms, thus facilitating the local accumulation of polar regions on the bilayer interface (see Fig. S4 in Supplementary Material). This demonstrates the dual role of trehalose: on the bilayer surface, trehalose can alter the H-bond distribution, thus inducing hydrophobic regions for palmitate to penetrate the bilayer, while in the aqueous phase, trehalose can interact with palmitate and prevent it from approaching the bilayer surface. These two competing processes help us to understand why the experimental measurements have shown that trehalose at high concentrations (>0.13 mM) is detrimental to HepG2 cells. At high trehalose concentrations, the bilayer surface is significantly modified by trehalose such that hydrophobic regions are more accessible for palmitate to penetrate the bilayer.

Embedded palmitate in bilayers

Thus far, we have found that a palmitate molecule can penetrate into the bilayer core within a short time (<40 ns). Although systems with more than one palmitate were also considered, their dynamics and properties contrast. This is because hydrophobic/hydrophilic interactions between palmitate molecules induce aggregation with characteristics similar to micelles. The aggregation of palmitate molecules in the aqueous phase partially shields the hydrophobic tails, which in turn lessen the driving force for palmitate to penetrate the bilayer. Moreover, the time for a sufficient number of palmitate molecules to penetrate the bilayer would likely require simulations into the microsecond domain. Therefore, to overcome this limitation, we created several model bilayers with palmitate molecules embedded in the bilayer structure (see Simulation Details). Since the amount of palmitate varies depending on the cell type and the level of toxicity, we considered a range of palmitate concentrations (11–44 mol %; see Table 1 for more details). To be consistent with previous analysis, the total number of lipids remained the same.

The following sections describe the global effect of palmitate embedded in the lipid bilayers (Systems 5–8 in Table 1). Since the bilayer surface was allowed to expand or contract as palmitate molecules are added into the bilayer, a correlation was established between the palmitate concentration and the bilayer surface area. As shown in Fig. S5, the total area per leaflet increases almost linearly with increasing palmitate concentration. This is seen because palmitate occupies an additional volume within the bilayer and, due to its alignment with the lipid tails, the bilayer expands in the lateral dimensions. An approximate area per lipid and palmitate can be determined using the criteria suggested by Edholm and Nagle, which deals specifically with heterogeneous systems (86). Although the bilayers considered here are multicomponent systems (POPC, POPE, and palmitate), for simplification, the lipids are grouped as one component and palmitate as the other. The area per molecule can be obtained from

$$\frac{A_{\text{total}}(x_{\text{palmitate}})}{N_{\text{lipid}}} = a_{\text{lipid}}(x_{\text{palmitate}}) + \frac{x_{\text{palmitate}}}{(1 - x_{\text{palmitate}})} a_{\text{palmitate}}(x_{\text{palmitate}}), \tag{3}$$

where A_{total} is the total area per leaflet; $x_{\text{palmitate}}$ is the mole fraction of palmitate in the bilayer; N_{lipid} is the total number of lipids per leaflet; and a_{lipid} and $a_{\text{palmitate}}$ are the area per lipid and area per palmitate, respectively. By plotting $A_{\text{total}}(x_{\text{palmitate}})/N_{\text{lipid}}$ versus $x_{\text{palmitate}}/(1 - x_{\text{palmitate}})$, as shown in Fig. 8 *a*, a_{lipid} and $a_{\text{palmitate}}$ can be determined from the *y*-intercept and slope, respectively. This analysis resulted in an average area per lipid and area per palmitate of ~0.576 and 0.071 nm^2, respectively. Our result for mixed 1:1 POPC/POPE systems is in the range of the experimental area per lipid for pure POPC (~0.64 nm^2) and POPE (~0.56 nm^2) bilayers at 300 K (87,88).

To further investigate the global effect of palmitate inside the membrane, a two-dimensional Voronoi tessellation analysis (89) was conducted on the equilibrium bilayer structure for systems containing palmitate (Systems 1 and 5–8 in Table 1). For the analysis considered, the Voronoi plane was defined by the position of carbonyl carbon atoms of the lipid and palmitate molecules, as these were located at about the same depth in the bilayer. The result of a Voronoi tessellation

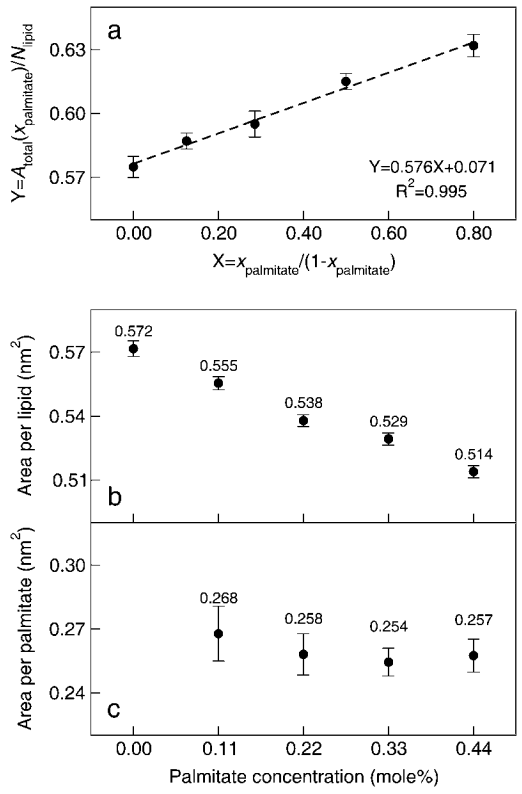

FIGURE 8 (*a*) Average area per leaflet and palmitate concentration. Dashed line is a linear regression of the data (fitted equation and correlation coefficient are shown). Error bars are estimated standard deviation of the trajectories collected over 50 ns. Plots *b* and *c* show the average area per lipid and palmitate obtained from Voronoi tessellation analysis for the corresponding lipid bilayers containing palmitate. Error bars are estimated standard error of the mean area of Voronoi polygons (see Fig. S6 in Supplementary Material).

analysis is a plot representing the spatial distribution of the molecules in the bilayer (see the Supplementary Material for a more detailed account of the Voronoi tessellation analysis done). In particular, the Voronoi plots show a random and disorder arrangement of the lipids and palmitate in the bilayer. Another useful property obtained from Voronoi plots is the area occupied by the lipid and palmitate molecules (calculated from the area of the polygons), as shown in Fig. 8, *b* and *c*, respectively. We see from the results in the figure that the area per lipid decreases with increasing palmitate concentration, whereas the area per palmitate remains constant, within statistical uncertainty. This demonstrates that palmitate, a fatty acid molecule with a long hydrocarbon tail, is laterally incompressible within the bilayer and its presence in the bilayer decreases the void space between the lipid molecules, and consequently decreases the average area per lipid. These observations are consistent with the reduced membrane fluidity (see Fig. 4) caused by the ordering induced by palmitate in the bilayer. We should also note that the average areas obtained from the Voronoi analysis differ from those based on the Edholm and Nagle method (Fig. 8 *a*), with exception of the pure bilayer where the estimate area per lipid are ~0.576 and ~0.572 nm^2, respectively. We believe the Voronoi tessellation analysis provides a more reliable estimate of the areas because it accounts for structural changes of the molecules in the bilayer and it links the structure from the simulations to the DSC measurements.

To investigate the local effect of palmitate embedded in the membranes, the lateral expansion of the bilayers is constrained (see Simulation Details). This is intended to mimic the local accumulation of palmitate in the bilayer. Fig. 9 demonstrates a significant change in bilayer structure after 44 mol % of palmitate is embedded into the bilayer. Unlike the global effect of palmitate embedded into the bilayer shown in Fig. 9 *b*, straight lipid tails with tilted arrangements are observed at higher palmitate concentrations (Fig. 9 *c*). This is related to the ordered lipid phase, which has been shown to be detrimental to cells by limiting their transport activities (90,91), binding sites for pathogens and toxins (92–94), and possibly the cause of palmitate-induced toxicity. As the palmitate concentration decreases, the arrangement of the

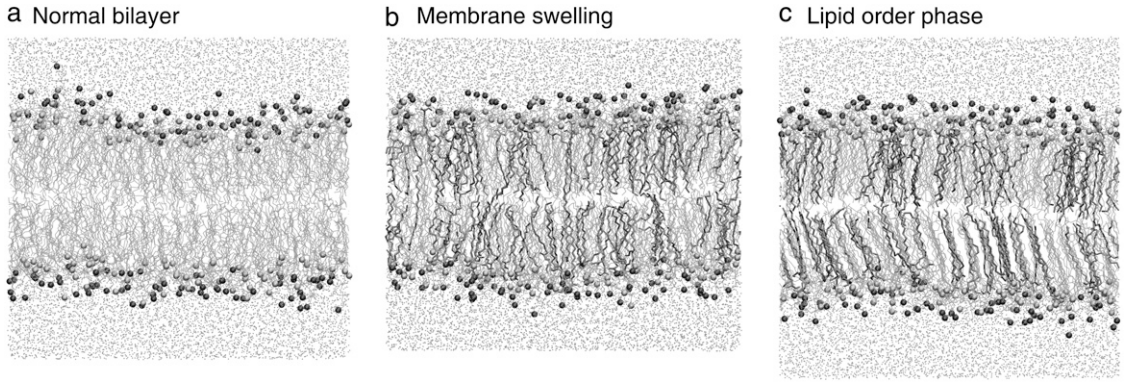

FIGURE 9 Snapshots of bilayer structures with (44 mol %) and without palmitate. (*a*) No palmitate is embedded in the bilayer. (*b*) The bilayer is allowed to expand as more palmitate molecules are embedded in the bilayer. (*c*) The bilayer is constraint in the lateral directions as more palmitate molecules are embedded in the bilayer. Dark gray molecules in the bilayer are palmitate. Compositions are described in Table 1.

lipid tails become more random as observed in Fig. 9 *a*, thus restoring the bilayer to its normal structure.

According to results shown in Fig. 8, it is implied that each palmitate molecule occupies a specific volume within the bilayer. This suggests that the structure of the lipid tails in the vicinity of the palmitate molecules can be significantly altered. Fig. 10 shows the lipid tail order parameter for Systems 5–8. As seen in the figure, there is an increase in the order parameter of the lipid tails as the palmitate concentration increases. One reason for this behavior is the additional volume occupied by the palmitate molecules, forcing the surrounding lipid molecules to become highly packed, resulting in a more ordered structure. Mechanistically, the area per headgroup remains relatively the same, despite the palmitate concentration; however, the area per lipid chain reduces significantly because palmitate occupies the void spaces that exist between the lipid chains. Since the lipid chains become more ordered (gel state) at the current state, it would require a higher temperature to transform them into a more disorder state (liquid-crystalline state). Therefore, our results demonstrated that the presence of palmitate increases the phase transition temperature of mixed 1:1 POPC/POPE bilayers.

Because the palmitate molecules are embedded in the bilayer at random, we are unable to quantify the local order parameter near each palmitate molecule, and as such, an average order parameter for the entire leaflet is reported. Note that the aggregation of palmitate within the bilayer cannot be captured within the timescale considered. However, the results do demonstrate swelling of the bilayers (see Fig. 9 *b*), which may eventually cause the bilayer structure to rupture or fuse with other cells, as reported by several experimental studies (51–53). Fig. 9 shows the changes to the bilayer structure caused by the addition of palmitate for the cases where the bilayer freely expands and remains constrained as palmitate is embedded in the bilayer (all bilayers contain the same number of palmitate in each leaflet, a condition needed to prevent distortion of the simulation box). As seen from the structures, the increase in the ordering of the lipid tails is related to the mixing of lipid and fatty acid components, where straight chain fatty acid exhibits higher order parameters. Since the ordering of the lipid tails is directly related to the phase transition, the simulation results agree well with the DSC measurements for DOPC liposomes containing palmitate, EPR measurements of HepG2 cells exposed to palmitate (see previous section), and other related experiments (81,82), all of which showed an increase in the phase-transition temperature with increasing palmitate concentration. In comparison to the effect of cholesterol on membranes, another predominant component in animal cells, our simulation results from the local and global effects of palmitate embedded within the membranes agree well with previous simulations of fully hydrated bilayers containing cholesterol, where increasing ordering of the lipids in the membrane is observed (95–98).

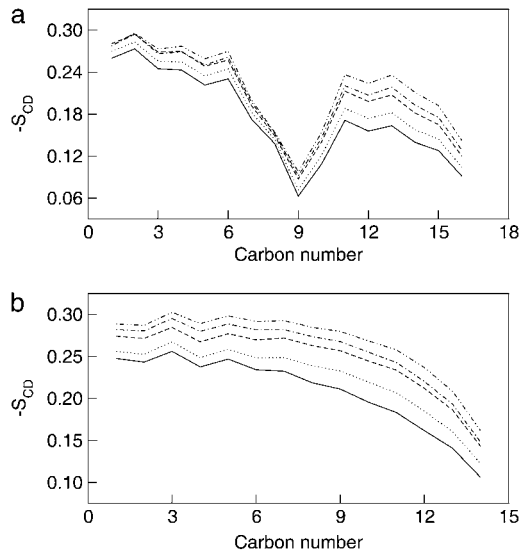

FIGURE 10 Deuterium order parameter for (*a*) monounsaturated and (*b*) saturated tails of POPC and POPE at 310 K. Lines correspond to: System 1 (*solid*), System 5 (*dot*), System 6 (*dash*), System 7 (*dot-dash*), and System 8 (*dot-dot-dash*).

DISCUSSION

FFAs are known to play important roles in the development of many hepatic disorders. A number of studies have shown that elevated levels of fatty acids are important mediators of lipotoxicity and can impair cellular functions and/or cause cell death (99). Others have found that the negative effect of FFA-induced toxicity may be reduced or alleviated by the addition of unsaturated fatty acids, antioxidants, or, as of more recently, disaccharides. To evaluate whether palmitate-induced toxicity can be reduced by adding trehalose, we exposed HepG2 cells to palmitate alone or a combination of trehalose and palmitate. As demonstrated from our experiment (Figs. 1 and 2), cells exposed to palmitate resulted in a significant amount of LDH and H_2O_2 released into the medium, indicating cell death or compromised cellular membrane. With increasing trehalose concentration, reduced amount of LDH released is observed in the presence of palmitate, up to ~13 mM, an optimal concentration for HepG2 cells. Furthermore, a significant reduction in H_2O_2 released is observed for these cells. To provide insight into the biochemical and biophysical processes altered by the presence of palmitate in HepG2 cells and to interpret these results from a molecular level, we studied the effect of palmitate and trehalose on model cell membranes (lipid bilayers) using molecular dynamic simulations.

Based on the results obtained from the simulations, we have demonstrated a potential mechanism by which palmitate incorporates into the bilayer and the binding of trehalose to palmitate through hydrogen bonding that may prevent palmitate from reaching the cell membrane and being taken

up. The incorporation process of palmitate into the bilayer may be similar to that in the detergent effect, where FFAs solubilize membrane components and create holes in the membrane. However, because the simulations are limited to nanosecond timescale and the solubilization of the membrane in the detergent effect process may occur in microseconds to seconds, we are unable to determine at the present time whether the detergent effect is actually the mechanism governing the toxicity by palmitate. Based on the results obtained from previous studies, trehalose has been shown to bind preferentially to the bilayer surface (72–74,77). This suggests that the hydrogen bonding between trehalose (up to a certain concentration) and the phospholipid components may prevent the formation of pores, thus preserving the normal membrane function and structure.

Modification of the membrane lipid composition may alter the membrane fluidity and in turn affect cellular function (100,101). As palmitate molecules are embedded within the membrane, it is observed from the EPR measurements that the membrane fluidity is significantly decreased (see Fig. 3). This phenomenon can be explained by many factors. First, palmitate is hydrophobic in nature and by exposing it to cell membranes, palmitate is most likely dissolving into the membrane, thus reducing the membrane fluidity. Second, as palmitate can be metabolized into phospholipid components of cell membranes, these additional components can cause an increase in the packing between the lipids, consequently decreasing the membrane fluidity (100,101). Last, since H_2O_2 and *OH are present in cultured cells exposed to palmitate, it has been reported that unsaturated phospholipids are oxidized into fragment of saturated hydrocarbons with various headgroup functionalities, some of which are highly toxic to cells (102–105). Although, the oxidation of unsaturated lipids generally results in an increase in fluidity and permeability of the membrane (106–109), the remaining fragments inside the membrane, which are hydrophobic in nature, can reduce the membrane fluidity. In this study, we found that palmitate decreased the cellular membrane fluidity of HepG2 cells. In support, a previous study found that palmitate enrichment in HepG2 cells results in decreased membrane fluidity, as demonstrated by higher fluorescence polarization of 1,6-diphenyl-1,3,5-hexatriene (46). This was expected, since others have shown that fatty acids incorporated into the membrane disrupted the bilayer structure and changed the lipid phase-transition temperature (81,82). We have observed similar results: increasing the concentration of palmitate increases the phase-transition temperature of DOPC.

CONCLUSIONS

In this study, we performed a series of experimental and computational measurements to gain insight into how trehalose interacts with HepG2 cells in the presence of palmitate. Experimentally, we found that healthy HepG2 cells exposed to palmitate resulted in a significant amount of LDH and H_2O_2 released into the medium, indicating cell death or compromised cellular membrane. Furthermore, it is observed from EPR measurements that the membrane fluidity is significantly decreased in the presence of palmitate, especially in the bilayer core region. The leading hypotheses for the observed results are:

1. Palmitate dissolves into the membrane, thus reducing the membrane fluidity.
2. Palmitate metabolizes into phospholipid components of cell membranes, thus increasing the packing between the lipids.
3. The remaining fragments of oxidized lipids inside the membrane (oxidized by H_2O_2 and *OH), which are hydrophobic in nature, reduce the membrane fluidity.

The computational component of this study is aimed at interpreting and understanding the experimental results, providing knowledge at the molecular level into the role of palmitate and trehalose in the toxicity of HepG2 cells. As illustrated by the results, the computation analyses confirmed that palmitate can dissolve into the bilayers within a short time. As the palmitate concentration in the bilayer increased, the order parameter of the lipid tails increased, which was consistent with the experimental results showing reduced membrane fluidity. The ordering of the lipid tails was due to the additional volume occupied by the palmitate molecules, forcing the surrounding lipid molecules to become highly packed, resulting in a more ordered structure. The local effect of palmitate embedded in the bilayer was also considered. The simulation results yielded a highly order bilayer structure with the lipid tails in a tilted arrangement. These results agreed well with DSC measurements for DOPC liposomes containing palmitate and EPR measurements of HepG2 cells exposed to palmitate. Furthermore, we verified that the direct interactions of trehalose and palmitate in the medium through hydrogen bonding potentially hinder palmitate from dissolving into the bilayer. The binding of palmitate to trehalose seems beneficial to cell membranes; however, we have also discovered from our mixed bilayer model that trehalose can potentially modify the bilayer surface by altering the surface hydrogen-bond distribution, thus inducing hydrophobic regions for palmitate to penetrate the bilayer.

SUPPLEMENTARY MATERIAL

To view all of the supplemental files associated with this article, visit www.biophysj.org.

DSC and EPR measurements were graciously provided by Dr. Neil Wright in the Department of Mechanical Engineering and Dr. John L. McCracken in the Department of Chemistry, respectively, at Michigan State University. Computational resources were provided by Virginia Tech Advanced Research Computing (System X).

This work was funded in part by the Michigan State University Foundation, the National Science Foundation (grant No. BES 0425821), and the National Institutes of Health (grant No. 1R01GM079688-01).

REFERENCES

1. Clandinin, M. T., S. Cheema, C. J. Field, M. L. Garg, J. Venkatraman, and T. R. Clandinin. 1991. Dietary fat: exogenous determination of membrane structure and cell function. *FASEB J.* 5:2761–2769.
2. Galli, C., and F. Marangoni. 1997. Recent advances in the biology of $n-6$ fatty acids. *Nutrition.* 13:978–985.
3. Yamashita, A., T. Sugiura, and K. Waku. 1997. Acyltransferases and transacylases involved in fatty acid remodeling of phospholipids and metabolism of bioactive lipids in mammalian cells. *J. Biochem.* (*Tokyo*). 122:1–16.
4. Andrade, L. N., T. M. de Lima, R. Curi, and A. M. Castrucci. 2005. Toxicity of fatty acids on murine and human melanoma cell lines. *Toxicol. In Vitro.* 19:553–560.
5. Lima, T. M., C. C. Kanunfre, C. Pompeia, R. Verlengia, and R. Curi. 2002. Ranking the toxicity of fatty acids on Jurkat and Raji cells by flow cytometric analysis. *Toxicol. In Vitro.* 16:741–747.
6. Maedler, K., G. A. Spinas, D. Dyntar, W. Moritz, N. Kaiser, and M. Y. Donath. 2001. Distinct effects of saturated and monounsaturated fatty acids on β-cell turnover and function. *Diabetes.* 50:69–76.
7. El-Assaad, W., J. Buteau, M. L. Peyot, C. Nolan, R. Roduit, S. Hardy, E. Joly, G. Dbaibo, L. Rosenberg, and M. Prentki. 2003. Saturated fatty acids synergize with elevated glucose to cause pancreatic β-cell death. *Endocrinology.* 144:4154–4163.
8. Kong, J. Y., and S. W. Rabkin. 2000. Palmitate-induced apoptosis in cardiomyocytes is mediated through alterations in mitochondria: prevention by cyclosporin A. *Biochim. Biophys. Acta Mol. Cell Biol. L.* 1485:45–55.
9. Sparagna, G. C., D. L. Hickson-Bick, L. M. Buja, and J. B. McMillin. 2000. A metabolic role for mitochondria in palmitate-induced cardiac myocyte apoptosis. *Am. J. Physiol. Heart C.* 279:H2124–H2132.
10. Dashti, N., Q. Feng, and F. A. Franklin. 2000. Long-term effects of *cis* and *trans* monounsaturated (18:1) and saturated (16:0) fatty acids on the synthesis and secretion of apolipoprotein A-I- and apolipoprotein B-containing lipoproteins in HepG2 cells. *J. Lipid Res.* 41: 1980–1990.
11. Ji, J., L. Zhang, P. Wang, Y. M. Mu, X. Y. Zhu, Y. Y. Wu, H. Yu, B. Zhang, S. M. Chen, and X. Z. Sun. 2005. Saturated free fatty acid, palmitic acid, induces apoptosis in fetal hepatocytes in culture. *Exp. Toxicol. Pathol.* 56:369–376.
12. Srivastava, S., and C. Chan. 2007. Hydrogen peroxide and hydroxyl radicals mediate palmitate-induced cytotoxicity to hepatoma cells: relation to mitochondrial permeability transition. *Free Radic. Res.* 41:38–49.
13. Listenberger, L. L., X. Han, S. E. Lewis, S. Cases, R. V. Farese, Jr., D. S. Ory, and J. E. Schaffer. 2003. Triglyceride accumulation protects against fatty acid-induced lipotoxicity. *Proc. Natl. Acad. Sci. USA.* 100: 3077–3082.
14. Dobrzyn, A., and J. M. Ntambi. 2005. The role of stearoyl-CoA desaturase in the control of metabolism. *Prostaglandins Leukot. Essent. Fatty Acids.* 73:35–41.
15. Borradaile, N. M., X. Han, J. D. Harp, S. E. Gale, D. S. Ory, and J. E. Schaffer. 2006. Disruption of endoplasmic reticulum structure and integrity in lipotoxic cell death. *J. Lipid Res.* 47:2726–2737.
16. Alexander, J. J., A. Snyder, and J. H. Tonsgard. 1998. Omega-oxidation of monocarboxylic acids in rat brain. *Neurochem. Res.* 23:227–233.
17. Sanders, R. J., R. Ofman, F. Valianpour, S. Kemp, and R. J. Wanders. 2005. Evidence for two enzymatic pathways for ω-oxidation of dodecanoic acid in rat liver microsomes. *J. Lipid Res.* 46:1001–1008.
18. Listenberger, L. L., D. S. Ory, and J. E. Schaffer. 2001. Palmitate-induced apoptosis can occur through a ceramide-independent pathway. *J. Biol. Chem.* 276:14890–14895.
19. Lu, Z.-H., Y.-M. Mu, B.-A. Wang, X.-L. Li, J.-M. Lu, J.-Y. Li, C.-Y. Pan, T. Yanase, and H. Nawata. 2003. Saturated free fatty acids, palmitic acid and stearic acid, induce apoptosis by stimulation of ceramide generation in rat testicular Leydig cell. *Biochem. Biophys. Res. Commun.* 303:1002–1007.
20. Goodman, D. S. 1958. The interaction of human erythrocytes with sodium palmitate. *J. Clin. Invest.* 37:1729–1735.
21. Spector, A. A. 1975. Fatty acid binding to plasma albumin. *J. Lipid Res.* 16:165–179.
22. Pande, S. V., and J. F. Mead. 1968. Inhibition of enzyme activities by free fatty acids. *J. Biol. Chem.* 243:6180–6185.
23. Reaven, P., S. Parthasarathy, B. J. Grasse, E. Miller, F. Almazan, F. H. Mattson, J. C. Khoo, D. Steinberg, and J. L. Witztum. 1991. Feasibility of using an oleate-rich diet to reduce the susceptibility of low-density lipoprotein to oxidative modification in humans. *Am. J. Clin. Nutr.* 54:701–706.
24. Hart, C. M., M. P. Gupta, and V. Evanoff. 1997. Oleic acid reduces oxidant stress in cultured pulmonary artery endothelial cells. *Exp. Lung Res.* 23:405–425.
25. Toborek, M., Y. W. Lee, R. Garrido, S. Kaiser, and B. Hennig. 2002. Unsaturated fatty acids selectively induce an inflammatory environment in human endothelial cells. *Am. J. Clin. Nutr.* 75:119–125.
26. Li, Z., S. Srivastava, S. Mittal, X. Yang, L. Sheng, and C. Chan. 2007. A three stage integrative pathway search (TIPS) framework to identify toxicity relevant genes and pathways. *BMC Bioinformatics.* 8:202.
27. Kinter, M., D. R. Spitz, and R. J. Roberts. 1996. Oleic acid incorporation protects cultured hamster fibroblasts from oxygen-induced cytotoxicity. *J. Nutr.* 126:2952–2959.
28. Natali, F., L. Siculella, S. Salvati, and G. V. Gnoni. 2007. Oleic acid is a potent inhibitor of fatty acid and cholesterol synthesis in c6 glioma cells. *J. Lipid Res.* 48:1966–1975.
29. Crowe, J. H., L. M. Crowe, and S. A. Jackson. 1983. Preservation of structural and functional activity in lyophilized sarcoplasmic reticulum. *Arch. Biochem. Biophys.* 220:477–484.
30. Crowe, J. H., L. M. Crowe, and D. Chapman. 1984. Preservation of membranes in anhydrobiotic organisms: the role of trehalose. *Science.* 223:701–703.
31. Leslie, S. B., E. Israeli, B. Lighthart, J. H. Crowe, and L. M. Crowe. 1995. Trehalose and sucrose protect both membranes and proteins in intact bacteria during drying. *Appl. Environ. Microbiol.* 61:3592–3597.
32. Wolkers, W. F., N. J. Walker, F. Tablin, and J. H. Crowe. 2001. Human platelets loaded with trehalose survive freeze-drying. *Cryobiology.* 42:79–87.
33. Elbein, A. D., Y. T. Pan, I. Pastuszak, and D. Carroll. 2003. New insights on trehalose: a multifunctional molecule. *Glycobiology.* 13: 17r–27r.
34. Chen, Q., and G. G. Haddad. 2004. Role of trehalose phosphate synthase and trehalose during hypoxia: from flies to mammals. *J. Exp. Biol.* 207:3125–3129.
35. Oku, K., M. Kurose, M. Kubota, S. Fukuda, M. Kurimoto, Y. Tujisaka, A. Okabe, and M. Sakurai. 2005. Combined NMR and quantum chemical studies on the interaction between trehalose and dienes relevant to the antioxidant function of trehalose. *J. Phys. Chem. B.* 109:3032–3040.
36. Herdeiro, R. S., M. D. Pereira, A. D. Panek, and E. C. A. Eleutherio. 2006. Trehalose protects *Saccharomyces cerevisiae* from lipid peroxidation during oxidative stress. *Biochim. Biophys. Acta Gen. Subj.* 1760:340–346.
37. Benaroudj, N., D. H. Lee, and A. L. Goldberg. 2001. Trehalose accumulation during cellular stress protects cells and cellular proteins from damage by oxygen radicals. *J. Biol. Chem.* 276:24261–24267.
38. Cirelli, N., P. Lebrun, C. Gueuning, J. Delogne-Desnoeck, A.-M. Vanbellinghen, G. Graff, and S. Meuris. 2001. Physiological concentrations of albumin stimulate chorionic gonadotrophin and placental lactogen release from human term placental explants. *Hum. Reprod.* 16:441–448.
39. Boden, G., X. Chen, E. Capulong, and M. Mozzoli. 2001. Effects of free fatty acids on gluconeogenesis and autoregulation of glucose production in type 2 diabetes. *Diabetes.* 50:810–816.

40. Mensink, M., E. E. Blaak, M. A. van Baak, A. J. Wagenmakers, and W. H. Saris. 2001. Plasma free fatty acid uptake and oxidation are already diminished in subjects at high risk for developing type 2 diabetes. *Diabetes*. 50:2548–2554.
41. Skowronski, R., C. B. Hollenbeck, B. B. Varasteh, Y. D. Chen, and G. M. Reaven. 1991. Regulation of non-esterified fatty acid and glycerol concentration by insulin in normal individuals and patients with type 2 diabetes. *Diabet. Med.* 8:330–333.
42. Woerle, H. J., E. Popa, J. Dostou, S. Welle, J. Gerich, and C. Meyer. 2002. Exogenous insulin replacement in type 2 diabetes reverses excessive hepatic glucose release, but not excessive renal glucose release and impaired free fatty acid clearance. *Metabolism*. 51:1494–1500.
43. Haak, R. A., L. M. Ingraham, R. L. Baehner, and L. A. Boxer. 1979. Membrane fluidity in human and mouse Chediak-Higashi leukocytes. *J. Clin. Invest.* 64:138–144.
44. Squier, T. C., D. J. Bigelow, and D. D. Thomas. 1988. Lipid fluidity directly modulates the overall protein rotational mobility of the Ca-ATPase in sarcoplasmic reticulum. *J. Biol. Chem.* 263:9178–9186.
45. Tsuda, K., Y. Kinoshita, K. Kimura, I. Nishio, and Y. Masuyama. 2001. Electron paramagnetic resonance investigation on modulatory effect of 17β-estradiol on membrane fluidity of erythrocytes in postmenopausal women. *Arterioscler. Thromb. Vasc. Biol.* 21:1306–1312.
46. Kuo, P., M. Weinfeld, and J. Loscalzo. 1990. Effect of membrane fatty acyl composition on LDL metabolism in HepG2 hepatocytes. *Biochemistry*. 29:6626–6632.
47. Madden, T. D., M. B. Bally, M. J. Hope, P. R. Cullis, H. P. Schieren, and A. S. Janoff. 1985. Protection of large unilamellar vesicles by trehalose during dehydration: retention of vesicle contents. *Biochim. Biophys. Acta Biomembr.* 817:67–74.
48. Womersley, C., P. S. Uster, A. S. Rudolph, and J. H. Crowe. 1986. Inhibition of dehydration-induced fusion between liposomal membranes by carbohydrates as measured by fluorescence energy-transfer. *Cryobiology*. 23:245–255.
49. Hoekstra, F. A., W. F. Wolkers, J. Buitink, E. A. Golovina, J. H. Crowe, and L. M. Crowe. 1997. Membrane stabilization in the dry state. *Comp. Biochem. Physiol. A*. 117:335–341.
50. Richieri, G. V., A. Anel, and A. M. Kleinfeld. 1993. Interactions of long-chain fatty acids and albumin: determination of free fatty acid levels using the fluorescent probe ADIFAB. *Biochemistry*. 32:7574–7580.
51. Raz, A., and A. Livne. 1973. Differential effects of lipids on the osmotic fragility of erythrocytes. *Biochim. Biophys. Acta*. 311:222–229.
52. Massenburg, D., and B. R. Lentz. 1993. Poly(ethylene glycol)-induced fusion and rupture of dipalmitoylphosphatidylcholine large, unilamellar extruded vesicles. *Biochemistry*. 32:9172–9180.
53. Burgess, S. W., D. Massenburg, J. Yates, and B. R. Lentz. 1991. Poly(ethylene glycol)-induced lipid mixing but not fusion between synthetic phosphatidylcholine large unilamellar vesicles. *Biochemistry*. 30:4193–4200.
54. Crowe, J. H., B. D. McKersie, and L. M. Crowe. 1989. Effects of free fatty acids and transition temperature on the stability of dry liposomes. *Biochim. Biophys. Acta Biomembr.* 979:7–10.
55. Tieleman, D. P., and H. J. C. Berendsen. 1998. A molecular dynamics study of the pores formed by *Escherichia coli* OmpF porin in a fully hydrated palmitoyloleoylphosphatidylcholine bilayer. *Biophys. J.* 74: 2786–2801.
56. Tieleman, D. P., L. R. Forrest, M. S. P. Sansom, and H. J. C. Berendsen. 1998. Lipid properties and the orientation of aromatic residues in OmpF, Influenza M2, and alamethicin systems: molecular dynamics simulations. *Biochemistry*. 37:17554–17561.
57. Leekumjorn, S., and A. K. Sum. 2007. Molecular characterization of gel and liquid-crystalline structures of fully hydrated POPC and POPE bilayers. *J. Phys. Chem. B*. 111:6026–6033.
58. Ryckaert, J. P., and A. Bellemans. 1975. Molecular dynamics of liquid normal-butane near its boiling-point. *Chem. Phys. Lett.* 30:123–125.
59. Berger, O., O. Edholm, and F. Jähnig. 1997. Molecular dynamics simulations of a fluid bilayer of dipalmitoylphosphatidylcholine at full hydration, constant pressure, and constant temperature. *Biophys. J.* 72:2002–2013.
60. Jorgensen, W. L., and J. Tirado-Rives. 1988. The OPLS potential function for proteins. Energy minimizations for crystals of cyclic peptides and crambin. *J. Am. Chem. Soc.* 110:1657–1666.
61. Essex, J. W., M. M. Hann, and W. G. Richards. 1994. Molecular dynamics simulation of a hydrated phospholipid-bilayer. *Philos. T. Roy. Soc. B*. 344:239–260.
62. Chiu, S. W., M. Clark, V. Balaji, S. Subramaniam, H. L. Scott, and E. Jakobsson. 1995. Incorporation of surface tension into molecular dynamics simulation of an interface: a fluid phase lipid bilayer membrane. *Biophys. J.* 69:1230–1245.
63. Damm, W., A. Frontera, J. Tirado-Rives, and W. L. Jorgensen. 1997. OPLS all-atom force field for carbohydrates. *J. Comput. Chem.* 18: 1955–1970.
64. van Gunsteren, W. F., and H. J. C. Berendsen. 1987. GROMOS-87 Manual. Biomos BV, AG Groningen, Nijenborgh, The Netherlands.
65. Berendsen, H. J. C., J. P. M. Postma, W. F. van Gunsteren, J. Hermans, and B. Pullman. 1981. Intermolecular Forces. Reidel, Dordrecht, The Netherlands.
66. Leekumjorn, S., and A. K. Sum. 2006. Molecular simulation study of structural and dynamic properties of mixed DPPC/DPPE bilayers. *Biophys. J.* 90:3951–3965.
67. Darden, T., D. York, and L. Pedersen. 1993. Particle mesh Ewald: an $N\cdot \log(N)$ method for Ewald sums in large systems. *J. Chem. Phys.* 98:10089–10092.
68. Essman, U., L. Perera, M. L. Berkowitz, T. Darden, H. Lee, and L. G. Pedersen. 1995. A smooth particle mesh Ewald method. *J. Chem. Phys.* 103:8577–8593.
69. Berendsen, H. J. C., D. van der Spoel, and R. van Drunen. 1995. GROMACS: a message-passing parallel molecular dynamics implementation. *Comput. Phys. Commun.* 91:43–56.
70. Lindahl, E., B. Hess, and D. van der Spoel. 2001. GROMACS 3.0: a package for molecular simulation and trajectory analysis. *J. Mol. Model.* 7:306–317.
71. Virginia Tech. Terascale Computing Facility. http://www.tcf.vt.edu.
72. Sum, A. K., R. Faller, and J. J. de Pablo. 2003. Molecular simulation study of phospholipid bilayers and insights of the interactions with disaccharides. *Biophys. J.* 85:2830–2844.
73. Pereira, C. S., R. D. Lins, I. Chandrasekhar, L. C. G. Freitas, and P. H. Hünenberger. 2004. Interaction of the disaccharide trehalose with a phospholipid bilayer: a molecular dynamics study. *Biophys. J.* 86:2273–2285.
74. Villarreal, M. A., S. B. Díaz, E. A. Disalvo, and G. G. Montich. 2004. Molecular dynamics simulation study of the interaction of trehalose with lipid membranes. *Langmuir*. 20:7844–7851.
75. Doxastakis, M., A. K. Sum, and J. J. de Pablo. 2005. Modulating membrane properties: the effect of trehalose and cholesterol on a phospholipid bilayer. *J. Phys. Chem. B*. 109:24173–24181.
76. Pereira, C. S., and P. H. Hunenberger. 2006. Interaction of the sugars trehalose, maltose and glucose with a phospholipid bilayer: a comparative molecular dynamics study. *J. Phys. Chem. B*. 110:15572–15581.
77. Leekumjorn, S., and A. K. Sum. 2006. Molecular investigation of the interactions of trehalose with lipid bilayers of DPPC, DPPE and their mixture. *Mol. Simul.* 32:219–230.
78. Rudolph, A. S., and J. H. Crowe. 1985. Membrane stabilization during freezing: the role of two natural cryoprotectants, trehalose and proline. *Cryobiology*. 22:367–377.
79. Hyvönen, M. T., K. Oorni, P. T. Kovanen, and M. Ala-Korpela. 2001. Changes in a phospholipid bilayer induced by the hydrolysis of a phospholipase A_2 enzyme: a molecular dynamics simulation study. *Biophys. J.* 80:565–578.
80. Knecht, V., A. E. Mark, and S. J. Marrink. 2006. Phase behavior of a phospholipid/fatty acid/water mixture studied in atomic detail. *J. Am. Chem. Soc.* 128:2030–2034.

81. Eliasz, A. W., D. Chapman, and D. F. Ewing. 1976. Phospholipid phase transitions. Effects of *n*-alcohols, *n*-monocarboxylic acids, phenylalkyl alcohols and quaternary ammonium compounds. *Biochim. Biophys. Acta. Biomembranes*. 448:220–230.
82. Mabrey, S., and J. M. Sturtevant. 1977. Incorporation of saturated fatty acids into phosphatidylcholine bilayers. *Biochim. Biophys. Acta Lipids Lipid Metabol*. 486:444–450.
83. Brady, J. W., and R. K. Schmidt. 1993. The role of hydrogen bonding in carbohydrates: molecular dynamics simulations of maltose in aqueous solution. *J. Phys. Chem.* 97:958–966.
84. Skibinsky, A., R. M. Venable, and R. W. Pastor. 2005. A molecular dynamics study of the response of lipid bilayers and monolayers to trehalose. *Biophys. J*. 89:4111–4121.
85. Venable, R. M., A. Skibinsky, and R. W. Pastor. 2006. Constant surface tension molecular dynamics simulations of lipid bilayers with trehalose. *Mol. Simul.* 32:849–855.
86. Edholm, O., and J. F. Nagle. 2005. Areas of molecules in membranes consisting of mixtures. *Biophys. J*. 89:1827–1832.
87. König, B., U. Dietrich, and G. Klose. 1997. Hydration and structural properties of mixed lipid/surfactant model membranes. *Langmuir*. 13:525–532.
88. Rand, R. P., and V. A. Parsegian. 1989. Hydration forces between phospholipid bilayers. *Biochim. Biophys. Acta Rev. Biomembranes*. 988:351–376.
89. Shinoda, W., and S. Okazaki. 1998. A Voronoi analysis of lipid area fluctuation in a bilayer. *J. Chem. Phys.* 109:1517–1521.
90. Thilo, L., H. Trauble, and P. Overath. 1977. Mechanistic interpretation of influence of lipid phase-transitions on transport functions. *Biochemistry*. 16:1283–1290.
91. Welti, R., D. A. Rintoul, F. Goodsaid-Zalduondo, S. Felder, and D. F. Silbert. 1981. Gel phase phospholipid in the plasma membrane of sterol-depleted mouse LM cells. Analysis by fluorescence polarization and x-ray diffraction. *J. Biol. Chem.* 256:7528–7535.
92. Herreros, J., T. Ng, and G. Schiavo. 2001. Lipid rafts act as specialized domains for tetanus toxin binding and internalization into neurons. *Mol. Biol. Cell.* 12:2947–2960.
93. Fantini, J., N. Garmy, R. Mahfoud, and N. Yahi. 2002. Lipid rafts: structure, function and role in HIV, Alzheimer's and prion diseases. *Expert Rev. Mol. Med.* 2002:1–22.
94. Lafont, F., and F. G. van der Goot. 2005. Bacterial invasion via lipid rafts. *Cell. Microbiol.* 7:613–620.
95. Smondyrev, A. M., and M. L. Berkowitz. 1999. Molecular dynamics simulation of DPPC bilayer in DMSO. *Biophys. J*. 76:2472–2478.
96. Chiu, S. W., E. Jakobsson, and H. L. Scott. 2001. Combined Monte Carlo and molecular dynamics simulation of hydrated lipid-cholesterol lipid bilayers at low cholesterol concentration. *Biophys. J*. 80:1104–1114.
97. Róg, T., and M. Pasenkiewicz-Gierula. 2006. Cholesterol effects on a mixed-chain phosphatidylcholine bilayer: a molecular dynamics simulation study. *Biochimie*. 88:449–460.
98. Cournia, Z., G. M. Ullman, and J. C. Smith. 2007. Differential effects of cholesterol, ergosterol and lanosterol on a dipalmitoyl phosphatidylcholine membrane: a molecular dynamics simulation study. *J. Phys. Chem. B*. 111:1786–1801.
99. Unger, R. H., and Y. T. Zhou. 2001. Lipotoxicity of β-cells in obesity and in other causes of fatty acid spillover. *Diabetes*. 50(Suppl 1):S118–S121.
100. Awad, A. B., and A. A. Spector. 1976. Modification of the fatty acid composition of Ehrlich ascites tumor cell plasma membranes. *Biochim. Biophys. Acta Biomembr*. 426:723–731.
101. Burns, C. P., D. G. Luttenegger, D. T. Dudley, G. R. Buettner, and A. A. Spector. 1979. Effect of modification of plasma membrane fatty acid composition on fluidity and methotrexate transport in L1210 murine leukemia cells. *Cancer Res*. 39:1726–1732.
102. Girotti, A. W. 1998. Lipid hydroperoxide generation, turnover, and effector action in biological systems. *J. Lipid Res*. 39:1529–1542.
103. Aldini, G., P. Granata, M. Orioli, E. Santaniello, and M. Carini. 2003. Detoxification of 4-hydroxynonenal (HNE) in keratinocytes: characterization of conjugated metabolites by liquid chromatography/electrospray ionization tandem mass spectrometry. *J. Mass Spectrom.* 38:1160–1168.
104. Hoff, H. F., J. O'Neil, Z. P. Wu, G. Hoppe, and R. L. Salomon. 2003. Phospholipid hydroxyalkenals—biological and chemical properties of specific oxidized lipids present in atherosclerotic lesions. *Arterioscler. Thromb. Vasc*. 23:275–282.
105. Reis, A., M. R. Domingues, F. M. Amado, A. J. Ferrer-Correia, and P. Domingues. 2005. Separation of peroxidation products of diacylphosphatidylcholines by reversed-phase liquid chromatography-mass spectrometry. *Biomed. Chromatogr*. 19:129–137.
106. Chatterjee, S. N., and S. Agarwal. 1988. Liposomes as membrane model for study of lipid peroxidation. *Free Radic. Biol. Med*. 4: 51–72.
107. Goldstein, R. M., and G. Weissmann. 1977. Effects of the generation of superoxide anion on permeability of liposomes. *Biochem. Biophys. Res. Commun*. 75:604–609.
108. Mandal, T. K., and S. N. Chatterjee. 1980. Ultraviolet- and sunlight-induced lipid peroxidation in liposomal membrane. *Radiat. Res*. 83: 290–302.
109. Kunimoto, M., K. Inoue, and S. Nojima. 1981. Effect of ferrous ion and ascorbate-induced lipid peroxidation on liposomal membranes. *Biochim. Biophys. Acta*. 646:169–178.